Lab on a Chip

Miniaturisation for chemistry, physics, biology, & bioengineering

www.rsc.org/loc

Volume 9 | Number 22 | 21 November 2009 | Pages 3165–3312

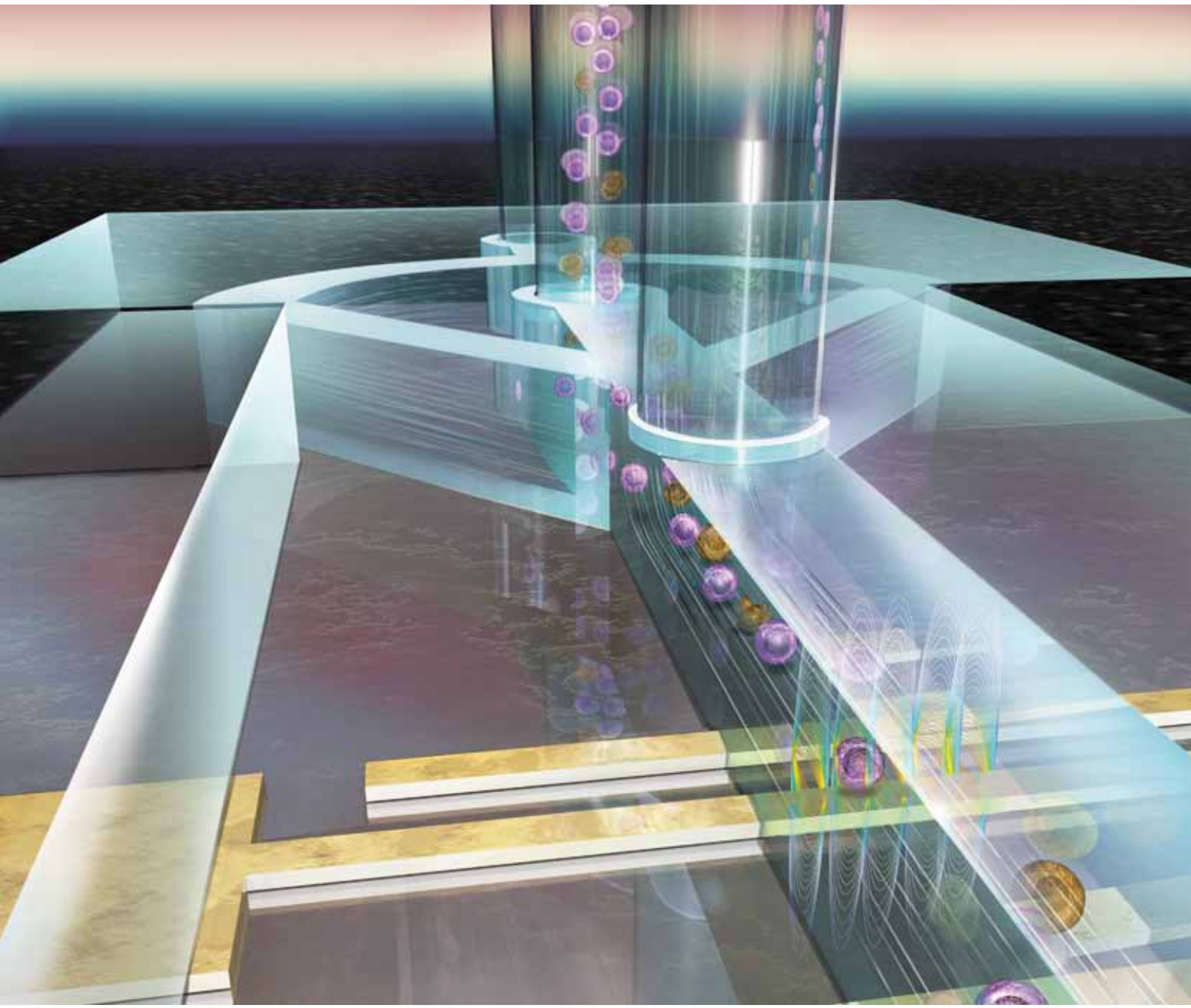

ISSN 1473-0197

Bashir
3D cytometry

Chang
3D (bio)particle sorter

Ren
Water toxicity testing

Hosokawa
Rapid SNP genotyping

RSC Publishing

1473-0197(2009)9:22;1-V

A robust electrical microcytometer with 3-dimensional hydrofocusing†

Nicholas Watkins,[a] Bala Murali Venkatesan,[a] Mehmet Toner,[c] William Rodriguez‡[d] and Rashid Bashir*[ab]

Received 24th June 2009, Accepted 24th August 2009
First published as an Advance Article on the web 22nd September 2009
DOI: 10.1039/b912214a

In this paper, we present a device to electrically count blood cell populations using an AC impedance interrogation technique in a microfabricated cytometer (microcytometer). Specifically, we direct our attention to obtaining the concentration of human CD4+ T lymphocytes (helper T cells), which is a necessary method to diagnose patients for HIV/AIDS and to give an accurate prognosis on the effectiveness of ARV (anti-retroviral) drug treatments. We study the effectiveness of a simple-to-fabricate 3-dimensional (3D) hydrodynamic focusing mechanism through fluidic simulations and corresponding experiments to increase the signal-to-noise ratio of impedance pulses caused by particle translocation and ensure lower variance in particle translocation height through the electrical sensing region. We found that the optimal 3D sheath flow settings result in a 44.4% increase in impedance pulse signal-to-noise ratio in addition to giving a more accurate representation of particle size distribution. Our microcytometer T cell counts closely with those found using an industry-standard flow cytometer for the concentration range of over three orders of magnitude and using a sample volume approximately the size of a drop of blood (~20 μL). In addition, our device displayed the capability to differentiate between live and dead/dying lymphocyte populations. This microcytometer can be the basis of a portable, rapid, inexpensive solution to obtaining live/dead blood cell counts even in the most resource-poor regions of the world.

Introduction

Cell counting is an essential practice in clinical immunology for the diagnosis and prognosis of disease, and has become especially important in the resource-poor regions of the world that have been crippled by the HIV/AIDS pandemic. Proper treatment of HIV/AIDS requires accurate helper T cell counts at regular intervals to monitor the health of a patient's immune system. With the recent push in global funding to make ARV (anti-retroviral) therapy available to all HIV-positive patients by 2010 (an estimated US $13.7 billion was invested in the AIDS response in 2008), it is crucial that affordable, easy-to-use, robust, and portable helper T cell counters be developed and distributed globally, especially in regions such as Sub-Saharan Africa, which contains 67% of the world's 33 million living with HIV.[1,2]

The additional information regarding a cell population's viability is a necessary enhancement to cell counting, as it provides a more accurate representation of a patient's condition by distinguishing live cells from dead/dying cells. One current live/dead cell counting method requires staining cells with a viability dye (*e.g.*, Trypan Blue or Propidium Iodide)—in addition to any other staining required to isolate the cell type of interest—and manually counting *via* hemocytometer under a microscope, which has a low test throughput, diminished accuracy inherent from human error, and is not portable. Flow cytometry is another method which minimizes these problems by analyzing cell populations using laser light scattering (LLS) and laser-induced fluorescence (LIF). Although flow cytometers have higher accuracy and throughput, they are not bringing the necessary penetration into the world's resource-poor regions because of their high initial cost (US $40000 to over $125000), periodic maintenance and repair costs, requirement of a trained technician, and lack of portability due to sheer size, weight, and fragile optical components.

There have been many reports of the development of cell counters using an affinity chromatography-based approach. Specifically, Cheng *et al.* reported a simple method to obtain T cell counts in micro-fluidic channels with differential shear flow.[3–5] T cells were selectively captured in a microfabricated channel using immobilized CD4 antibodies and then counted under a standard light or fluorescence microscope to obtain the concentration. This technique was subsequently enhanced by integrating impedance spectroscopy into the capture channel to monitor the cell lysates.[6] T cells from whole blood were captured on-chip and lysed in a low-conductivity buffer, releasing intracellular ions into the bulk solution, thereby changing its conductance, which increased proportionally with cell concentration. The authors were able to correlate cell concentration with channel

[a]*Department of Electrical and Computer Engineering, Micro and Nanotechnology Laboratory, University of Illinois, Urbana, IL, 61801, USA. E-mail: rbashir@illinois.edu; Fax: +1-217-244-6375; Tel: +1-217-333-3097*
[b]*Department of Bioengineering, University of Illinois, Urbana, IL, 61801, USA*
[c]*Surgical Services and Bio MEMS Resource Center, Massachusetts General Hospital, Harvard Medical School, Shiners Hospital for Children, Boston, MA, 02114, USA*
[d]*Partners AIDS Research Center, Massachusetts General Hospital and Division of AIDS, Harvard Medical School, Brigham and Women's Hospital, Boston, MA, 02115, USA*

† Electronic supplementary information (ESI) available: Supplementary information for Fig. 1 and Fig. 3. See DOI: 10.1039/b912214a

‡ Current Address: Daktari Diagnostics, Inc., Arlington, MA 02476, USA.

conductance with a detection sensitivity of 20 cells·μL^{-1} and eliminating the need of a microscope and manual cell counting.

The realization of a miniaturized cytometer would create a truly portable blood analysis system that would eliminate the human error factor and need for external equipment and contain the inherent accuracy and high sample throughputs found in larger bench-top flow cytometer systems. Much emphasis has been placed on converting the large, expensive, and complex flow cytometers and Coulter counters into their microfabricated counterparts. Some benefits of these microcytometers include: (1) they require much smaller volumes of blood or plasma and expensive reagents, (2) less expensive operation and maintenance costs, (3) mobile platforms that can go directly to a high-needs area, regardless of health care infrastructure, and (4) the realization of a closed, one-time-use device for the handling of blood and other biohazardous fluids. Many have investigated the miniaturization of optical flow cytometers,[7–13] but we have chosen the electrical interrogation method using the Coulter principle[14,15] to create a more streamlined, cost-effective, and mechanically robust solution for portable cellular analysis.

Microscale Coulter counters using the DC voltage interrogation method have been reported,[16–20] however, the use of an alternating voltage field is preferred over an electrostatic field since the alternating fields (1) prevent electrode destruction from Galvanic current heating effects for higher voltages in ionic solutions, (2) prevent fouling of electrodes by charged cellular debris, and (3) can use different frequencies to dynamically interrogate the different cellular components (DNA, cytoplasm, organelles, *etc.*). Ayliffe *et al.* first used the AC interrogation method on a microfabricated chip to perform impedance measurements of individual stationary cells in a microfabricated chip.[21] Cells were pulled through narrow channels *via* suction and strategically placed between 4 μm thick gold electrodes. An impedance analyzer was then used to determine the magnitude and phase of the cell's impedance at different frequencies. Sohn *et al.* developed a microfluidic device that measured the change in capacitance caused by cells flowing through an AC field region.[22] They found that the polarization response of a cell's negatively charged DNA would cause a change in the system's capacitance. This would support their findings of a positive linear relationship between the change in capacitance and a cell's DNA content. As a result, they could determine a cell's current growth phase. Several groups have simultaneously measured the impedance of mobile cells at multiple discrete frequencies.[23–26] Gawad *et al.* have investigated several AC impedance models to determine various cellular properties, such as cell size, membrane capacitance, cytoplasm resistance, and electrode double layer capacitance.[23,27] There have also been reports of combining both optical and electrical methods on-chip.[28,29] Wang *et al.* integrated a commercial metal oxide semiconductor field effect transistor (MOSFET) with optical fluorescence detection to determine the percent of CD4+ T cells among a total population of lymphocytes.[29] They have also created a similar system replacing the MOSFET with a two-stage differential amplification system.[30,31]

In this study, we investigated the reliability and accuracy of an electrical micro flow cytometer for the portable live/dead analysis of CD4+ T cells using the AC impedance technique coupled with 3D hydrodynamic focusing. We used the electrical sensing technique as it ensures simple fabrication and gives the greatest potential for cost-effective miniaturization. We investigated the optimal sheath and sample flow conditions through simulations and corresponding experiments to ensure consistent particle translocation height above the sensing electrodes. The 3D focusing mechanism required no additional microfabrication steps and was effective in causing particles to flow consistently close to the sensing electrodes, resulting in a 44.4% increase in the impedance pulse signal-to-noise ratio and a more accurate depiction of particle size distribution. We compared the helper T cell concentrations given by our device and those from a standard flow cytometer and found our device was accurate (R^2 = 0.95). We believe this design is capable as the back end for a total lab-on-a-chip system for the enumeration of different blood cell types for the diagnosis of various diseases.

Principle

Fig. 1(a) illustrates the concept of a microfabricated device with 3D hydrodynamic focusing that will be used to analyze blood cell populations. It is comprised of a hydrodynamic focusing region that manipulates cell position and an electrical interrogation region that counts individual cells. The electrical interrogation region is designed after the aforementioned Coulter principle. A low-frequency (50 kHz) AC voltage signal is applied across parallel, coplanar micro electrodes, resulting in parabolic current lines that extend upwards toward the top of the channel. A cell or other particle passing through this region will either enhance or block the current, depending on the relative conductivity of the particle to the surrounding medium. This will temporarily change the effective impedance of the sensing region, resulting in an impedance pulse with a width corresponding to the particle translocation time. In this study, cells are treated as non-conducting spheres at 50 kHz, which is well below the characteristic frequency, f_C, of a cell's membrane (>2–3 MHz).[32,33] Cell passage will increase the impedance of the sensing region similar to the polystyrene particles also used in this investigation. Therefore, particle size (or conversely, the volume of conductive buffer

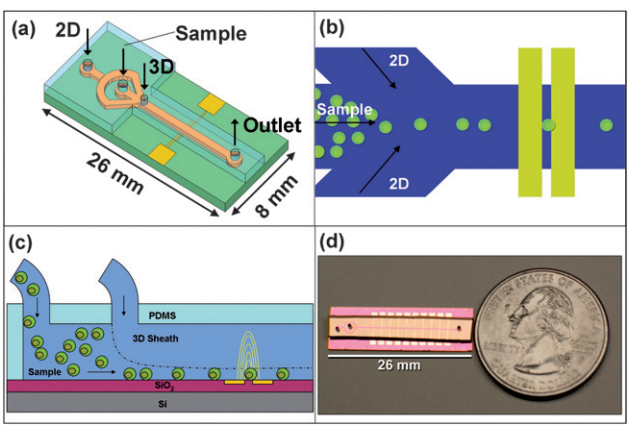

Fig. 1 Concept of electrical microcytometer with 3D focusing mechanism. (a) Chip-level view of the 3D hydrodynamic focusing and electrical sensing region (not drawn to scale). (b) The 2D sheaths force particles in the sample stream to flow in a single file manner and the (c) 3D sheath ensures the particles flow consistently close to the sensing electrodes. (d) Size comparison of chip to a quarter dollar.

displaced by the particle) will dominate the impedance pulse amplitude.

Hydrodynamic focusing is a simple but elegant mechanism used in flow cytometry to ensure accurate population analysis by forcing particles to flow in a single-file and spatially consistent manner through the sensing region. This reduces the possibility of coincidence events, where multiple particles simultaneously pass through the sensing region, and decreases signal inaccuracies from variance in particle translocation position.[34] Hydrodynamic focusing relies on the concept of laminar fluid flow where a fluid's viscous forces dominate its inertial forces, creating a predictable and stable flow in which multiple streams flow adjacently with little or no mixing. The low Reynolds number associated with microscale fluidic channels creates an ideal environment for laminar flow, even at relatively high fluid velocities (in our case, up to 26 $cm \cdot s^{-1}$ with a total flow rate of 100 $\mu L \cdot min^{-1}$). We take advantage of this property to ensure cells and other particles flow in a single file manner and consistently in close proximity to the sensing electrodes. Fig. 1(b) illustrates how we first force particles into a single-file line *via* lateral sheath flows. Although this 2D focusing mechanism greatly reduces the probability of coincidence events, the system still suffers inaccuracy from the variance of pulse amplitude from particles passing through the sensing region at varying heights.[23] To solve this problem, we subsequently use a third sheath to vertically confine the sample stream close to the sensing electrodes, completing the 3D focusing mechanism (Fig. 1(c)). This increases the impedance pulse signal-to-noise ratio by forcing cells to pass through the highest current line density nearest the electrodes. It also better represents the size distribution of a particle population by eliminating the variance in particle translocation height (*e.g.*, larger particle passing farther from electrodes may block the same amount of current as a smaller particle passing closer to the electrodes). Therefore, one can confidently assume pulse height is directly proportional to particle size.

An optimal sheath-to-sample flow rate ratio (R) is necessary to create a sample stream core that is the approximate dimensions of the cells or other particles of interest. R is generally defined as

$$R = \frac{F_{SHEATH}}{F_{SAMPLE}} \quad (1)$$

where, F_{SHEATH} and F_{SAMPLE} are the sheath and sample infusion flow rates, respectively. Specifically, R_{2D} represents the flow rate ratio of the laterally confining sheaths (split from same inlet) to the sample, while R_{3D} represents the flow rate ratio of the vertically confining sheath to the sample. We use simulations and experiments to optimize R_{2D} and R_{3D} for the enumeration of helper T cell concentrations.

Materials and methods

Microcytometer fabrication†

Standard photolithography and metal lift-off techniques were used to create recessed 300 nm Ti/Pt sensing electrodes on an oxidized Si substrate. Recesses were created by etching the SiO_2 with buffered HF acid (BHF) before metal deposition, and ensured optimal bonding of the fluidic layer (see below) by eliminating the abrupt step height of the electrodes.

The microfluidic channels were created by a standardized and rapid technique using a thick negative photoresist (SU-8; Microchem Corp., Newton, MA) and a biocompatible polymer, Poly(dimethylsiloxane) (PDMS; Dow Corning, Midland, MI). In this process, SU-8 is used to create a 32 μm-thick negative mold of the channel structure; unpolymerized PDMS is then poured over the mold and cured, resulting in a positive image of the microchannels. Cured PDMS dies were cut out and holes corresponding to the 2D and 3D sheath inlets, sample inlet, and outlet were punched out using customized syringe needles. A hermetic seal between the PDMS and substrate was formed by oxidizing both with O_2 plasma in a barrel etcher followed by quick alignment of channels to electrodes and bonding. Microbore tubing was inserted into the three inlets and sealed with epoxy to create a fluidic pathway between the chip and three Harvard syringe pumps (Harvard Apparatus, Holliston, MA), enabling independent control over each inlet infusion rate.

Electrical impedance sensing setup

Fig. 2 illustrates the experimental setup used to hydrodynamically manipulate and electrically interrogate cell and particle populations. The SR 850 lock-in amplifier (Stanford Research Systems, Inc., Sunnyvale, CA) was used to apply a 4 V (rms) internally-referenced 50 kHz sinusoidal signal across the resistor R and the platinum electrodes (14 μm wide, 7 μm gap). The value of R was chosen to match the impedance value of the channel sensing region at 50 kHz in order to facilitate the highest sensitivity when a cell or particle perturbs it. An Agilent 4284 LCR meter (Agilent Technologies, Inc., Palo Alto, CA) was used to find the impedance spectrum of the electrodes in PBS for the 10^2 to 10^6 Hz frequency range, and an R value of 10 kΩ was obtained. Real (X) and Imaginary (Y) impedance signals were exported from the lock in amplifier and recorded in binary format on a computer running NI LabVIEW *via* a PCI-6221 DAQ card (National Instruments, Austin, TX). Matlab (The MathWorks, Natick, MA) was used to convert the NI binary file

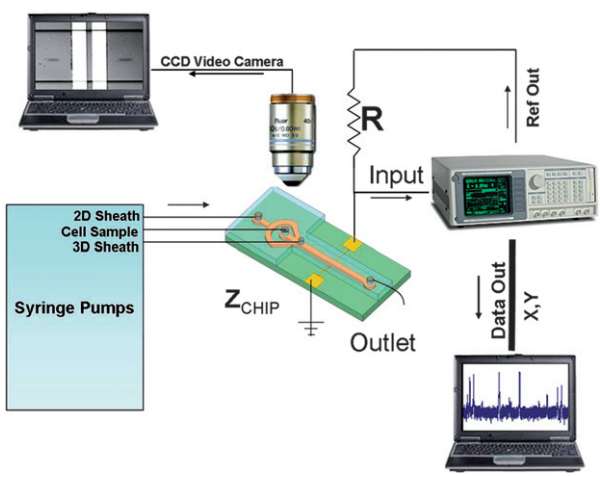

Fig. 2 Experimental setup: syringe pumps control sample and sheath flows through the sensing region, which is connected to the external circuit *via* micro-manipulators (not shown).

into a text format to be read in by the Axon Clampfit 10 software (Molecular Devices, Sunnyvale, CA). Clampfit was used to adjust the baseline of the impedance signal, filter out excess noise, and analyze the impedance pulses using the threshold search method. This method only records a pulse when its amplitude is at least the same as the trigger level (in our case, set as a multiplicative factor of the standard deviation of the noise of the baseline signal without cells or particles). Three syringe pumps were used to independently control the sample, 2D sheath, and 3D sheath inlet flow rates in order to facilitate and investigate the 3D hydrodynamic focusing of particles and cells. A sensitive Pixera Penguin 600CL CCD camera (Pixera Corporation, San Jose, CA) coupled to a Nikon Eclipse E600FN microscope (Nikon Instruments, Inc., Melville, NY) was used to observe cells and beads passing through the sensing region, ensuring particles were being focused and that impedance pulses were from particle passage.

Simulations of 2D and 3D focusing of sample stream

The FLUENT Computational Fluid Dynamics simulation package (ANSYS, Lebanon, NH) was used to find the optimal flow rate ratios between the sample inlet and each of the 2D and 3D sheath inlets. Experiments, described below, were performed to evaluate the accuracy of the 2D and 3D focusing simulations.

2D focusing of sample stream of Trypan Blue

The optimal R_{2D} was obtained experimentally by independently varying the infusion rates of the 2D sheath and sample inlet syringe pumps. Trypan Blue dye was infused into the sample inlet to distinguish the sample flow stream from the sheath flow streams. The sample stream width was precisely measured by analyzing micrographs taken using a digital video camera coupled to a microscope. This analysis was performed on a chip with a glass substrate to enhance the contrast of the sample stream *via* microscope backlight. No 3D sheath inlet was punched into the PDMS microfluidics layer.

3D focusing of polystyrene particles

The optimal 3D sheath flow rate ratio was experimentally found by focusing 7.32 μm polystyrene microparticles (Bangs Laboratories, Inc., Fishers, IN) and by varying R_{3D} and observing the change in the average and distribution of impedance pulse heights. R_{2D} was locked at the optimal ratio found in the 2D Trypan Blue experiment. The total flow rate was locked at a constant value to ensure constant bead velocity through the sensing region for all 3D flow ratios because it was found that the average pulse heights would decrease for increasing bead velocities (unpublished data). The shorter pulses in the time domain from faster bead velocities result in a broader spectrum of frequency components that are lower in amplitude; eventually, the higher frequency components are clipped out by the lock-in's low pass filter. The microbeads were diluted in phosphate buffered saline (PBS), sonicated for 5 minutes to reduce bead aggregates, and infused into the sample port at a flow rate of 4 $\mu L \cdot min^{-1}$ with a total flow rate (2D sheath + 3D sheath + sample) of 100 $\mu L \cdot min^{-1}$.

CD4+ T-lymphocyte concentration comparisons

It is imperative that the microfabricated chip can reliably provide cell counts that are comparable to the industry standard method of flow cytometry. In this study, we compared our device to the Becton Dickinson LSR II Flow Cytometer (Becton Dickinson, Franklin Lakes, NJ) by analyzing varying dilutions of cultured 8E5/LAV cells, a human lymphoblastic cell line from ATCC (Manassas, VA). Cells were cultured two to three times a week in RPMI-1640 media (ATCC) with 10% fetal bovine serum (Fetalplex, Gemini Bio-Products, West Sacramento, CA) and kept in a 5% CO_2 incubator at 37 °C. Various dilutions of the lymphoblasts were created by the following method. Approximately 10 mL of 8E5/LAV cell suspension was spun down into a pellet using an Eppendorf 5810R refrigerated centrifuge (Eppendorf International, Hamburg, Germany) at 4 °C and 200 × g for 10 minutes. The pellet was resuspended in PBS + 1% bovine serum albumin (BSA), pelleted a second time, and resuspended in 1 mL PBS + 1% BSA to obtain a high concentration of cells (5×10^6 mL^{-1}). A dilution series was then created to give concentrations ranging from 10^3 to 5×10^6 $cells \cdot mL^{-1}$. Cells were kept on ice during the entire experiment. Each dilution was then injected into the sample inlet *via* syringe pump at a rate of 4 $\mu L \cdot min^{-1}$ with the 2D and 3D sheath pumps infusing PBS at their respective optimal rates. Cell concentration was found by dividing the number of pulses by the known amount of sample volume flown during a 5 minute time period (20 μL total volume flown). The BD LSR II flow cytometer was then used to obtain the concentration of aliquots from the same dilutions. A known volume of a known concentration of FITC fluorescent beads (Bangs Laboratories) was mixed with each cell dilution. The beads were gated on the FITC channel with an event stop value of 10000 total beads. Cellular events were gated based on their forward scattering (FSC) and side scattering (SSC) characteristics. Cell concentrations were calculated by the ratio of cellular events to bead events, multiplied by the known concentration of counting beads.

Results and discussion

Optimal flow ratios for 2D and 3D focusing of particles

A 3D representation of the fabricated 200 μm wide and 32 μm high microchannels was constructed using hexahedral cells[35] (~175000) in the Gambit mesh generation software (ANSYS) and imported into FLUENT. A volume of fluid (VOF) multiphase model was constructed assuming laminar, incompressible, immiscible, and isothermal flows as well as a no-slip condition at all sidewalls. The optimal R_{2D} was obtained by performing multiple simulations with R_{2D} ranging from 1 to 16 with the 3D sheath flow velocity set to 0. After 2500 iterations, the sample stream width, W_S, was determined by measuring the width of cells which contain at least a 50% volume fraction of the fluid from the sample fluid.[36]

Fig. 3(a) illustrates a completed simulation with $R_{2D} = 8$, which gave a W_S of ~12 μm, an appropriate width for focusing blood cells. Experiments were performed to compare W_S dependence on R_{2D} from the simulation results using Trypan Blue dye to distinguish the sample flow stream from the sheath flow streams. 50% (v/v) Trypan Blue and DI water were infused

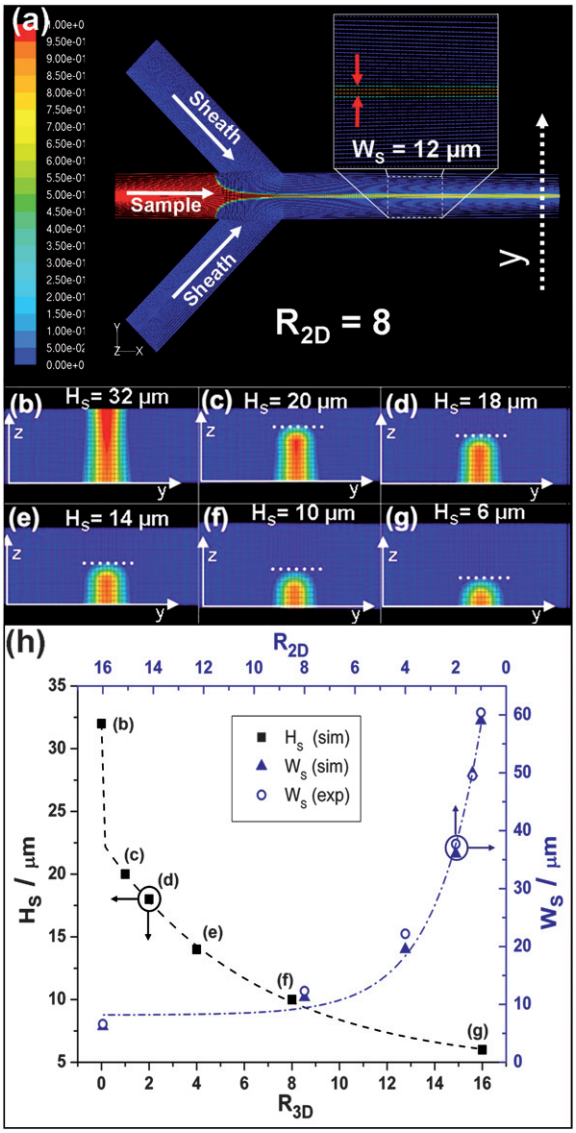

Fig. 3 (a) FLUENT simulation of 2D hydrofocusing of the sample stream for $R_{2D} = 8$, giving an optimal sample stream width of 12 μm. (b–g) Height profile of sample stream for R_{3D} values of 0, 1, 2, 4, 8 16, respectively; profile was taken parallel to the Y axis, as denoted in (a). (h, top and right axes) Comparison between experimental (open circles) and simulated (solid triangles) results for W_S for various R_{2D} values; dash-dot line represents exponential fitting of simulated data (R^2 = 0.992). (h, bottom and left axes) Sample stream height dependence on R_{3D} from simulations with labels linking points to corresponding simulations in (b–g); dashed line represents two-phase exponential association fitting ($R^2 = 0.999$).

into the sample and sheath inlet ports, respectively. Infusion rates for both sample and 2D sheath pumps were varied to match the flow rate ratios in the simulations. Micrographs were taken 30 s after changes in R_{2D} to ensure the system was stable. W_S values were obtained by comparing the dyed stream to the known channel width.† Fig. 3(h) shows the decaying exponential dependence of W_S on R_{2D} and the strong agreement between the experimental and simulated results. This consistency ensures that cells of particular size can be predictably focused into a single file line at the corresponding flow rate ratio.

The optimal R_{3D} was obtained through simulations by locking R_{2D} at 8, and varying R_{3D} from 1 to 16. Fig. 3(h) illustrates the decaying exponential dependence of sample stream height, H_S, on R_{3D}. Fig. 3(f) shows that an R_{3D} of 8 gave the optimal H_S of ~10 μm, creating a sample stream core with the same dimensions of blood cells. This size ensured cells and particles would stay in close proximity to the sensing electrodes but was large enough to keep them within the sample flow stream. Experiments were performed to test the accuracy of these simulations as well as the reliability of our 3D focusing mechanism. Polystyrene beads were injected into the sample inlet at identical R_{2D} and R_{3D} values to those tested in FLUENT, and 5 minutes of impedance data was recorded (20 μL). Clampfit was used to record and analyze pulses that were at least four times the standard deviation of the baseline noise. Fig. 4(a) illustrates how bead impedance pulses become more uniform with $R_{3D} = 8$, (iii), versus no 3D focusing, (ii), showing that the beads were indeed flowing closer to the electrodes at a higher consistency. This can be quantitatively reflected in the increase in mean and decrease in standard deviation of the pulse amplitude for a duration of 4 s from (ii) to (iii). Fig. 4(b) shows the percentage change, $\%\Delta\mu_Z$, in average pulse height for varying R_{3D} values and the corresponding percent change in standard deviations, $\%\Delta\sigma_Z$, for the entire 5 minutes of analysis. $\%\Delta\mu_Z$ is the normalized difference between average pulse height amplitudes for $R_{3D} > 0$ (μ_x) and $R_{3D} = 0$ (μ_0), and is defined as

$$\%\Delta\mu_Z = \frac{\mu_x - \mu_0}{\mu_0} \quad (2)$$

$\%\Delta\sigma_Z$ is calculated in the same way, but replacing μ_x and μ_0 with σ_x and σ_0, respectively. The positive correlation between pulse amplitude and R_{3D} for $R_{3D} = 1$ to 8 shows that the beads were successfully being manipulated to flow closer to the sensing electrodes and block a higher percentage of current. It was found that $R_{3D} = 8$ resulted in the largest increase of average pulse amplitude (44.4%) and largest decrease in pulse amplitude standard deviation (15.4%) versus no 3D focusing. $R_{3D} = 16$ resulted in a decrease in mean amplitude and increase in standard deviation most likely because the sample stream height was too small (~6 μm in simulations, Fig. 3(g)) to consistently contain the 7.32 μm particles. Its 30.8% increase in standard deviation over no 3D focusing ($R_{3D} = 0$) could be from the fact that many particles could not stay within the sample stream and were forced into the sheath at varying heights above the electrodes. Fig. 4(c) compares the pulse height distributions between beads undergoing no 3D focusing and optimal focusing ($R_{3D} = 8$). The differences between the pulse distributions show that the optimal 3D focusing of the particles results in a better representation of particle size distribution. In the case of no 3D focusing, the pulse distribution is of decaying exponential nature. Optimal focusing results in a Gaussian distribution, which is expected for the discrete-sized microparticles with a mean diameter. This eliminates pulse amplitude ambiguity caused by variance in particle translocation height above the sensing electrodes. Fig. 4(d) shows the pulse duration histogram for no 3D focusing and optimal 3D focusing. Optimal 3D focusing gives a larger average duration because particles are flowing closer to the electrodes, where the field line distribution covers more distance in the direction of particle flow. The 39.9% decrease in standard

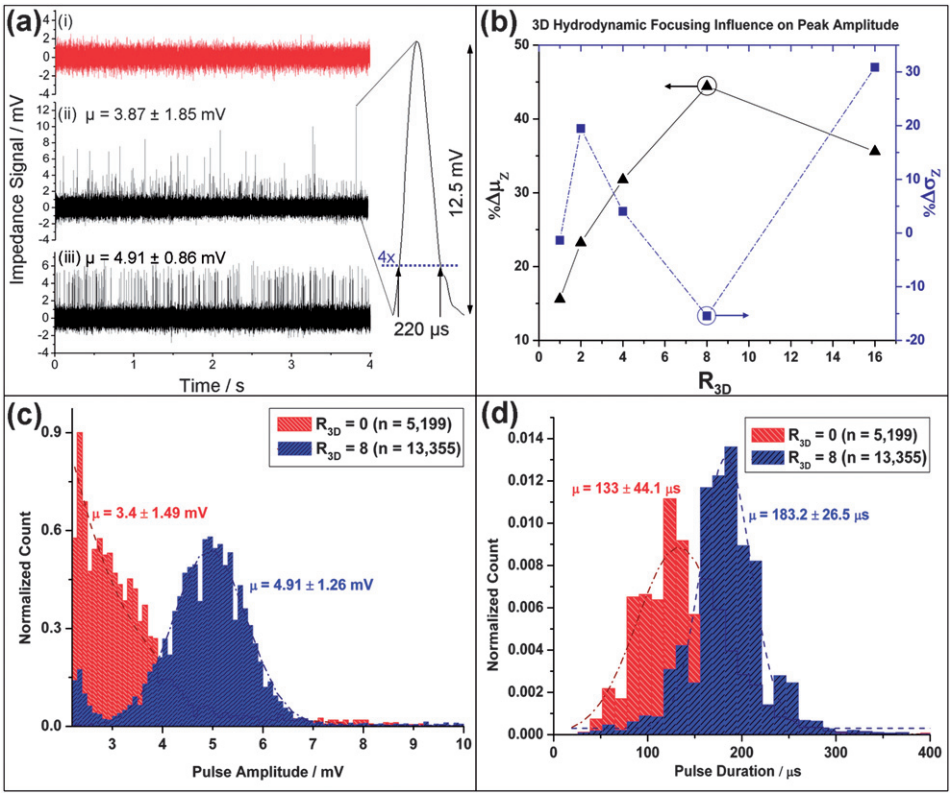

Fig. 4 Effect of 3D focusing of 7.32 μm polystyrene particles on electrical analysis. (a) (i) Baseline impedance signal (no beads), (ii) signal with beads and no 3D focusing ($R_{3D} = 0$) with pulse amplitude statistics for 4 s duration, and (iii) signal with beads and optimal 3D focusing ($R_{3D} = 8$) with pulse amplitude statistics. (a, inset) Magnification of a single impedance pulse and the concept of threshold analysis using a trigger that is four times the standard deviation of the noise in (i); pulse duration is calculated from the intersection of the pulse with the trigger, while pulse magnitude is simply the maximum height within the pulse duration. (b) Percent change in mean pulse magnitude, $\%\Delta\mu_Z$ (triangles, solid line), and standard deviation, $\%\Delta\sigma_Z$ (squares, dash-dot line), relative to $R_{3D} = 0$ for various R_{3D} values. Number of triggered events (R_{3D} value in parentheses): n = 5199 (0), n = 17157 (1), n = 11106 (2), n = 11869 (4), n = 13355 (8), and n = 3457 (16). (c) Pulse height distribution comparison between $R_{3D} = 0$ and $R_{3D} = 8$; statistics shown are from raw data; curve fitting is used to show how the distribution drastically changes from decaying exponential for $R_{3D} = 0$ ($R^2 = 0.95$) to Gaussian for $R_{3D} = 8$ ($R^2 = 0.97$). (d) Pulse duration (relative to 4x trigger level) distribution comparison between $R_{3D} = 0$ and $R_{3D} = 8$; statistics shown are from Gaussian curve fittings ($R^2 = 0.94$ for $R_{3D} = 0$ and $R^2 = 0.92$ for $R_{3D} = 8$). For both (c) and (d), an outline of the $R_{3D} = 0$ distribution is shown when it is overlapped by the $R_{3D} = 8$ distribution.

deviation at optimal focusing conditions further supports that the beads were translocating at a more consistent height above the electrodes.

T cell concentration comparison

T cell counts using the electrical micro cytometer were compared against the BD LSR II flow cytometer for concentrations ranging over three orders of magnitude (10^3 to 2×10^6 cells·mL^{-1}) with the majority of concentrations within the critical range of <500 cells·μL^{-1} for HIV/AIDS diagnostics. 20 μL of each sample was analyzed by the microcytometer under optimal 3D focusing conditions ($R_{2D} = R_{3D} = 8$). Clampfit was used to obtain each sample concentration by denoting a cellular event as a pulse that was at least five times the standard deviation of the baseline noise. As a control, aliquots from the same samples were then analyzed by the LSR II flow cytometer. Fig. 5 compares the LSR II data, (a), with that of the microcytometer, (b). The FSC histogram in Fig. 5(a) shows the cell size distribution found using the flow cytometer, which can be compared to the pulse height histogram of the electrical microcytometer in (b). There is a noticeable difference between the two histograms in that the FSC histogram contains a secondary peak, which denotes live cells. As previously mentioned, in impedance spectroscopy, cells are treated as non-conducting spheres at frequencies well below f_C. Frequencies higher than f_C effectively short the capacitance of the cell membrane *via* relaxation mechanisms (β-dispersion),[32] which allows for the investigation of the internal electrical characteristics of the cells such as cytoplasm conductivity and DNA content that could give more insight into whether a cell was alive or dead. In our case, the cells are treated as non-conducting spheres. Therefore, it was necessary to gate whole cells in the LSR II data for a fair comparison with the data from the electrical counter, as illustrated in the inset of Fig. 5(a).

The following is our logic in gating whole cells for the flow cytometry data. In flow cytometry, the magnitude of forward scattering depends proportionally on cell size and refractive index, while side scattering depends on the complexity of the

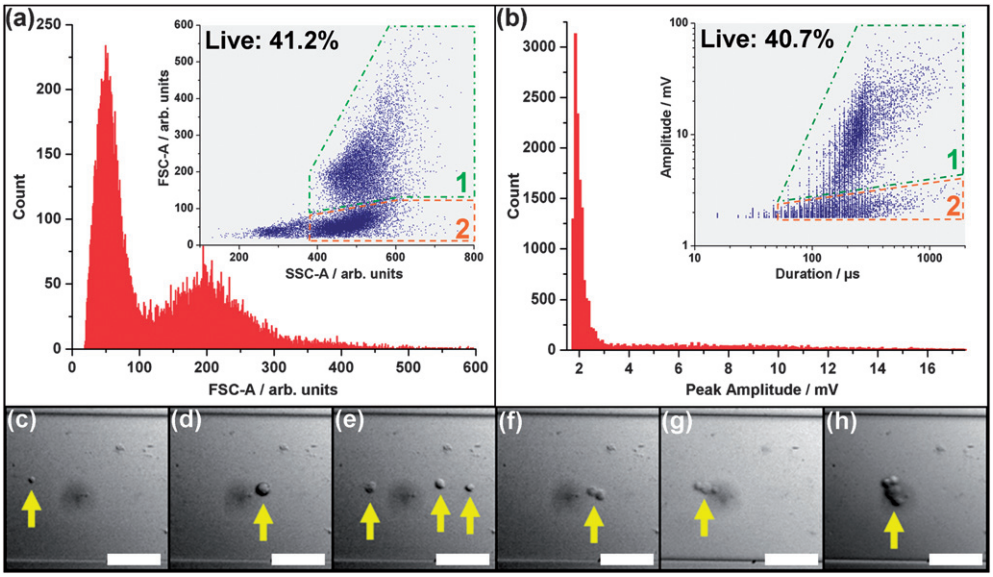

Fig. 5 Comparison between the analysis of aliquots from the same sample of helper T cells by flow cytometer and electrical microcytometer. (a) LSR II flow cytometer analysis; FSC histogram relates cell size distribution while the inset FSC *vs.* SSC scatter plot illustrates the two sub-populations of whole cells: living (region 1) and dead/dying (region 2). (b) Electrical microcytometer analysis; pulse amplitude histogram shows cell size distribution; inset scatter plot shows relationship between cell translocation time and peak amplitude, and distinguishes between live (region 1) and dead/dying (region 2) cells. The percent of live whole cells was calculated by dividing the number of events in region 1 by the total number of whole cells (regions 1 and 2). (c–h) Micrographs of focused helper T cells illustrating their large size variation: (c) healthy cell (8.7 µm in diameter), (d) dead/dying cell (18.2 µm), (e) multiple cells flowing in a single-file manner, and clumps of cells as (f) doublets, (g) triplets, and (h) quadruplets. White scale bars are 75 µm.

cell's interior (*e.g.*, granularity).[34] A whole cell that is dead or dying will have a compromised membrane, allowing surrounding media to enter, which effectively reduces the refractive index of the cell and the level of forward scattering. Side scattering will roughly remain unchanged between living and dead/dying cells because cellular contents still remain intact inside the membrane. Therefore, whole cellular events are gated on the entire FSC range and the limited SSC range (>∼375 arbitrary units) as depicted in regions 1 and 2 in the inset of Fig. 5(a).

The inset of Fig. 5(b) represents the relationship between impedance pulse height and pulse width (measured with respect to 5x trigger) for the microcytometer. It is interesting to note that we observed two different populations for cells analyzed by the electrical microcytometer, which could not be distinguished by the aforementioned pulse height histogram. The events in region 1 show a strong positive correlation between the peak amplitude and duration, which is expected for non-conducting spheres. However, the events in region 2 show a higher variance in duration over a smaller amplitude range. We postulate that these are dead or dying whole cells with compromised membranes or ionic channels. These cells cannot be modeled as non-conducting particles, as electrical conduction can take place within the cell, reducing the effective impedance of the cell. The large variance in duration in this region can be explained by the fact that the cells were undergoing apoptosis and increased in size. This will increase the translocation time of the cells, but will have little effect on pulse amplitude because of the cells' compromised membranes. Using this theory, we found that the fraction of live T cells found by the microcytometer matched closely with that of the LSR II flow cytometer for a aliquots from the same sample (40.7% *vs.* 41.2%, respectively). Fig. 5(c–h) illustrates how cell size can vary from 8.7 µm with a healthy T cell (c), to over twice as large during apoptosis (d), or even larger *via* clumping of multiple cells (f–h).

Fig. 6 shows the correlation of 13 concentration values found from the electrical microcytometer and the LSR II flow cytometer. Each point represents one particular dilution that was

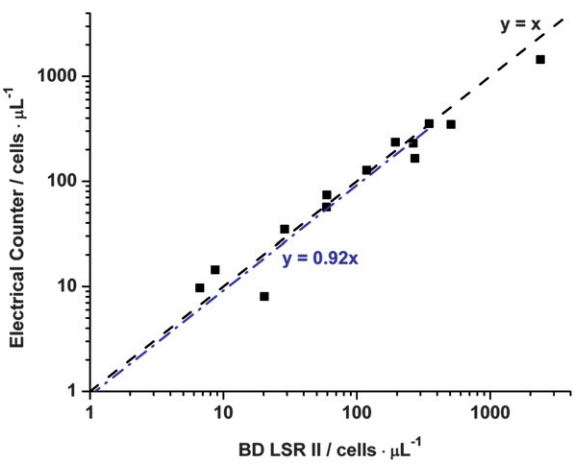

Fig. 6 Concentration comparison between the electrical counter and the LSR II flow cytometer for the full range of the 13 concentrations analyzed (10 to 2000 cells·µL^{-1}). The dash-dot line is a linear regression for the 11 samples ($R^2 = 0.95$) within the critical range (<500 cells·µL^{-1}) and indicates good correlation between the two methods. The dashed line denotes 1:1 correlation between both analysis methods.

measured by both methods. The microcytometer proved to perform well for the whole range of concentrations tested, especially in the critical concentration range of <500 cells·μL^{-1} ($n = 11$; $R^2 = 0.95$), even considering that measurements were taken from different aliquots of the same dilution and includes inherent pipetting error.

Conclusions

We have investigated a microfabricated AC impedance analysis system for the electrical counting of CD4+ T lymphocytes for point-of-care blood analysis. The two-stage 3D focusing mechanism was easily fabricated using a single microfluidics layer, and ensured cells and particles flowed in a single-file line and consistently close to the sensing electrodes. This not only enhanced the sensitivity of the device—giving CD4+ T lymphocyte counts comparable to an industry standard flow cytometer—but ensured accurate representation of the size distribution of the population, which can help differentiate among different cell types in heterogenous populations and aid in understanding cell growth cycles in homogenous populations. In addition, we found that it has the capability to differentiate between live cells and those with compromised membranes, providing the possibility of on-chip live/dead cell counts. A simple-to-use handheld device can be realized *via* a simplified chip or IC-based lock-in amplifier and a miniaturized pumping system. This design will provide an inexpensive and reliable back end to a totally autonomous blood cell counter which selectively isolates and subsequently counts a specific cell type for analysis of various diseases.

Acknowledgements

The authors would like to thank Dr. Yi-Shao Liu and Bobby Reddy, Jr., for their helpful comments during device fabrication. Partial support was provided by the United States Department of Homeland Security graduate student fellowship and from the National Institute of Biomedical Imaging and Bioengineering (BioMEMS Resource Center, P41 EB002503).

Notes and references

1 UNAIDS: *2008 Report on the Global AIDS Epidemic: Status of the Global HIV Epidemic*. http://data.unaids.org/pub/GlobalReport/2008/jc1510_2008_global_report_pp29_62_en.pdf. Accessed 25 April 2009.
2 UNAIDS: *What countries need: Investments needed for 2010 targets (2009)*. http://data.unaids.org/pub/Report/2009/20090210_investments_needed_2010_en.pdf. Accessed 24 April 2009.
3 X. Cheng, D. Irimia, M. Dixon, K. Sekine, U. Demirci, L. Zamir, R. Tompkins, W. Rodriguez and M. Toner, *Lab Chip*, 2007, **7**, 170.
4 X. Cheng, D. Irimia, M. Dixon, J. Ziperstein, U. Demirci, L. Zamir, R. Tompkins, M. Toner and W. Rodriguez, *JAIDS-J. Acq. Imm. Def.*, 2007, **45**(3), 257.
5 X. Cheng, A. Gupta, C. Chen, R. Tompkins, W. Rodriguez and M. Toner, *Lab Chip*, 2009, **9**, 1357.
6 X. Cheng, Y.-S. Liu, D. Irimia, U. Demirci, L. Yang, L. Zamir, W. Rodriguez, M. Toner and R. Bashir, *Lab Chip*, 2007, **7**, 746.
7 E. Altendorf, D. Zebert, M. Holl, P. Yager, *Transducers '97: 1997 International Conference on Solid-State Sensor and Actuators*, vol. 1, p. 531, Chicago, 1997.
8 T. Arakawa, Y. Shirasaki, T. Izumi, T. Aoki, H. Sugino, T. Funatsu and S. Shoji, *Meas. Sci. Technol.*, 2006, **17**, 3141.
9 A. Wolff, I. Perch-Nielsen, U. Larsen, P. Friis, G. Goranovic, C. Poulsen, J. Kutter and P. Telleman, *Lab Chip*, 2003, **3**, 22.
10 K. Takahashi, A. Hattori, I. Suzuki, T. Ichiki and K. Yasuda, *J. Nanobiotechnol.*, 2004, **2**(5).
11 C.-C. Lin, A. Chen and C.-H. Lin, *Biomed. Microdevices*, 2008, **10**, 55.
12 H. Chen and Y. Wang, *Microfluid. Nanofluid.*, 2009, **6**, 529.
13 X. Mao, S.-C. Lin, C. Dong and T. Huang, *Lab Chip*, 2009, **9**, 1583.
14 US Pat., 2 656 508, 1953.
15 W. H. Coulter, *Proceedings of National Electronics Conference*, vol. 12, p. 1034, Chicago, 1956.
16 K. Roberts, M. Parameswaran, M. Moore, R. Muller, *Proceedings of the 1999 IEEE Canadian Conference on Electrical and Computer Engineering*, Edmonton, Alberta, 1999.
17 M. Koch, A. Evans and A. Brunnschweiler, *J. Micromech. Microeng.*, 1999, **9**, 159.
18 D. Satake, H. Ebi, N. Oku, K. Matsuda, H. Takao, M. Ashiki and M. Ishida, *Sens. Actuators, B*, 2002, **83**, 77.
19 D. Lee, S. Yi and Y.-H. Cho, *J. Microelectromech. Syst.*, 2008, **17**(1), 139.
20 H. Chun, T. Chung, H. Kim, *Proceedings of the 26th Annual International Conference of the IEEE EMBS*, San Francisco, 2004.
21 H. Ayliffe, A. Frazier and R. Rabbitt, *J. Microelectromech. Syst.*, 1999, **8**(1), 50.
22 L. Sohn, O. Saleh, G. Facer, A. Beavis, R. Allan and D. Notterman, *Proc. Natl. Acad. Sci. U. S. A.*, 2000, **97**(20), 10687.
23 C. Fuller, J. Hamilton, H. Ackler, P. Krulevitch, B. Boser, A. Eldredge, J. Y. F. Becker, P. Gascoyne, *The 4th International Conference on Miniaturized Systems for Chemistry and Life Sciences (MicroTAS)*, Enschede, 2000.
24 S. Gawad, L. Schild and P. Renaud, *Lab Chip*, 2001, **1**, 76.
25 K. Cheung, S. Gawad and P. Renaud, *Cytometry, Part A*, 2005, **65A**, 124.
26 T. Sun, D. Holmes, S. Gawad, N. Green and H. Morgan, *Lab Chip*, 2007, **7**, 1034.
27 S. Gawad, K. Cheung, U. Seger, A. Bertsch and P. Renaud, *Lab Chip*, 2004, **4**, 241.
28 H. Morgan, D. Holmes and N. Green, *Curr. Appl. Phys.*, 2006, **6**(3), 367.
29 Y. Wang, Y. Kang, D. Xu, C. Chon, L. Barnett, S. Kalams, D. Li and D. Li, *Lab Chip*, 2008, **8**, 309.
30 X. Wu, C. Chon, Y. Wang, Y. Kang and D. Li, *Lab Chip*, 2008, **8**, 1943.
31 X. Wu, Y. Kang, Y. Wang, D. Xu, D. Li and D. Li, *Electrophoresis*, 2008, **29**(13), 2754.
32 H. Schwan, in *Advances in Biological and Medical Physics*, ed. J. H. Lawrence and C. A. Tobias, Academic, New York, 1957, vol. 5, p. 147.
33 H. Morgan, T. Sun, D. Holmes, S. Gawad and N. Green, *J. Phys. D: Appl. Phys.*, 2007, **40**, 61.
34 H. Shapiro, *Practical Flow Cytometry*, Wiley, Hoboken, NJ, 4th edn., 2006.
35 To avoid ambiguity, the "cells" referenced in this section refer to discrete volumes used in finite element modeling, unless otherwise noted.
36 The volume fraction of a cell is the percentage of cell volume that contains the phase of interest.

